ROYAL SOCIETY
OF CHEMISTRY

COMMUNICATION

Check for updates

Na[Mn$_{0.36}$Ni$_{0.44}$Ti$_{0.15}$Fe$_{0.05}$]O$_2$ predicted via machine learning for high energy Na-ion batteries†

Saaya Sekine,[a] Tomooki Hosaka, [ID][a] Hayato Maejima,[a] Ryoichi Tatara, [ID][a] Masanobu Nakayama [ID][b] and Shinichi Komaba*[a]

We optimize the composition of transition metal layered oxides for high energy Na-ion batteries using machine learning (ML) trained by our experimental data. The ML models predict their electrochemical performance and suggest promising compositions of quaternary Na[Ni,Mn,Fe,Ti]O$_2$. Accordingly, we synthesized Na[Mn$_{0.36}$Ni$_{0.44}$Ti$_{0.15}$Fe$_{0.05}$]O$_2$ which achieves a high energy density of 549 W h per kg of active material, agreeing with the predicted value.

Introduction

As renewable energy adoption increases, there is a significant demand for storing energy by using large-format stationary batteries. Although Li-ion batteries (LIBs) are favored for their high energy density, lithium resources are limited to only 24 ppm in the earth's crust and are unevenly distributed in the world,[1] which poses challenges for resource pricing and supply stability. Consequently, Na-ion batteries (SIBs) composed of cost-effective and abundant metals are attracting attention as next-generation batteries.[2]

Sodium-containing transition-metal layered oxides, employed as positive electrode materials for SIBs, have been studied since the 1970s and are recognized for forming a variety of crystal structures depending on the synthesis conditions and sodium content.[1,3–5] The primary structures formed via high-temperature crystallization are identified as O3- and P2-types.[6,7] Among these, the O3-type structure is notable for its high sodium content, which is essential for high capacity in Na-ion full cells.[8]

Beyond structural aspects, the composition also has a significant impact on electrochemical performance. Selection and ratio of transition metals affect their morphology, capacity, cycle performance, and rate capabilities.[9] Therefore, extensive studies have focused on the compositional optimization of sodium layered oxides.[10–12] In our group, a hard-working master-course student solely synthesized 27 samples of O3-type Na[Ni,Mn,Fe,Ti]O$_2$ and found that O3–Na$_{5/6}$[Mn$_{1/6}$Ni$_{1/3}$Ti$_{1/3}$Fe$_{1/6}$]O$_2$ demonstrates a well-balanced combination of energy density of positive electrode and capacity retention.[13] Due to the extensive range of potential compositional combinations for multi-element layered oxides, an efficient method for composition optimization is crucial to identify a positive electrode material that exhibits higher energy density and good cycle performance. In this context, machine learning (ML) methods based on experimental data accumulated over the decade[14] are expected to successfully predict battery performance from the composition.[15,16] While there have been studies employing ML to predict the electrochemical performance of various battery materials,[17,18] efforts to predict the electrochemical properties of layered oxides for SIBs have been notably limited. Furthermore, this method can significantly reduce the number of necessary experiments, optimize synthesis conditions, and even extract new insights from failed experiments, offering numerous advantages.[19]

In this study, we constructed a database of the O3-type transition metal layered oxides synthesized and evaluated in our group. Our dataset comprises the compositional information alongside the electrochemical data. Subsequently, we trained ML models using the database to predict discharge capacity, average discharge voltage, and capacity retention. In addition, an inverse analysis was performed to predict promising compositions. As a result, we have successfully developed a new material, Na[Mn$_{0.36}$Ni$_{0.44}$Ti$_{0.15}$Fe$_{0.05}$]O$_2$, which has the highest predicted energy density among the predicted compositions. Thus, this material was synthesized and evaluated in Na cells (Fig. 1).

Experimental

A database including 100 charge–discharge data of Na half cells of 68 different O3-type NaMeO$_2$ compositions evaluated in our

*a*Department of Applied Chemistry, Tokyo University of Science, Shinjuku, Tokyo 162-8601, Japan. E-mail: komaba@rs.tus.ac.jp

*b*Department of Life Science and Applied Chemistry, Nagoya Institute of Technology, 1-30 Gokisho, Showa, Nagoya, 466-8555, Japan

This journal is © The Royal Society of Chemistry 2024

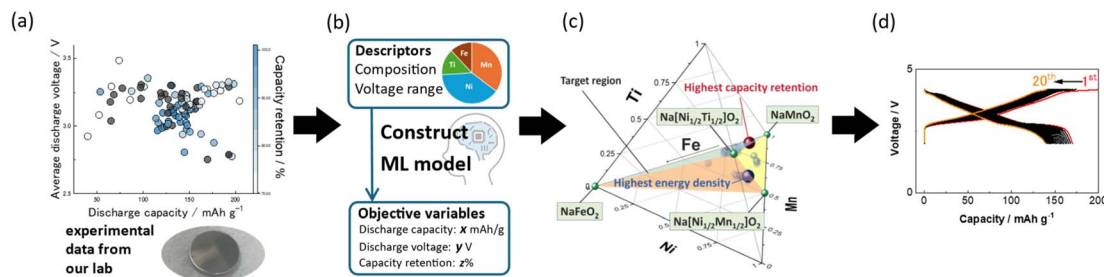J. Mater. Chem. A, 2024, 12, 31103–31107 | 31103

Fig. 1 The process of exploring new NaMeO$_2$ cathode materials for sodium-ion batteries using ML. (a) Experimental dataset utilized in this study, (b) construct machine learning model, (c) explore promising compositions, (d) experimentally verify the electrochemical properties of the resulting compositions.

group over the past 11 years was used (Fig. 1a, S1†). The larger number of charge–discharge data is because some materials are tested in different voltage ranges. The database includes the composition of NaMeO$_2$ (Me = Mn, Ni, Ti, Zn, Fe, Sn, Co, Mg, Cu, Al, W), upper and lower voltage limits of charge–discharge tests, initial discharge capacity, average discharge voltage, and capacity retention after 20 cycles. For capacity retention, the available data were of 68 Na half cells with different 47 compositions because we excluded some data with less than 20 cycles.

The compositions and upper and lower voltage limits were utilized as explanatory variables to predict the initial discharge capacity, the average initial discharge voltage, and the capacity retention after 20 cycles (Fig. 1b). The regression was performed with a series of ML algorithms, including Lasso (least absolute shrinkage and selection operator) regression, ridge regression, SVR (support vector machine regression), Kernel SVR, elastic net, partial least squares (PLS) regression, random forest, and LightGBM (Table S1†). The training data was 80% of the total data, and the rest 20% of the data was used as test data to verify the generalization ability using root mean squared error (RMSE).

The constructed model was used to search for promising compositions. To conduct an efficient search, multi-objective Bayesian optimization for energy density of positive electrode and capacity retention was employed. The method to calculate the energy density of positive electrode is initial discharge capacity (mA h g^{-1}) × average initial discharge voltage (V). In the search for promising compositions, the upper and lower voltage limits were fixed to 2.0 and 4.2 V, respectively. The

compositional range for optimization was limited in a quaternary phase diagram with end members of NaMnO$_2$, NaMnNiO$_2$, NaFeO$_2$, and NaNiTiO$_2$ (Fig. 1c).

The predicted promising sample of Na[Mn$_{0.36}$Ni$_{0.44}$Ti$_{0.15}$Fe$_{0.05}$]O$_2$ was prepared via a conventional solid-state method at 800 °C. For the electrochemical tests, R2032-type coin cells were assembled in an Ar-filled glove box. Constant-current charge/discharge tests were conducted at 25 °C at a current rate of 12.7 mA g^{-1} (Fig. 1d). The details are shown in the ESI.†

Results and discussion

A series of ML models were trained to predict discharge capacity, discharge voltage, and capacity retention from the compositional descriptors (molar fraction of metal ions) in NaMeO$_2$ with different ML algorithms (Table S1†). For all three target variables, the linear regression (Lasso, linear SVR, PLS, Ridge) model exhibited an underfitting, indicating the nonlinear relationship between the target variables (transition metal ratio and operating voltage) and the descriptors (electrochemical performance).[20] In contrast, random forest and LightGBM, which are decision tree based models, achieved good prediction abilities with low RMSE. LightGBM achieved the lowest RMSE of test data for initial discharge capacity, and random forest did it for discharge voltage and capacity retention (Table S1†). The best prediction models for discharge capacity and voltage showed RMSEs of 16 mA h g^{-1} and 0.058 V, corresponding to 11.1%, 1.2% of average relative error, respectively (Fig. S2,† 2a and b). In contrast, the capacity retention (random forest) exhibited an RMSE of 6.5%,
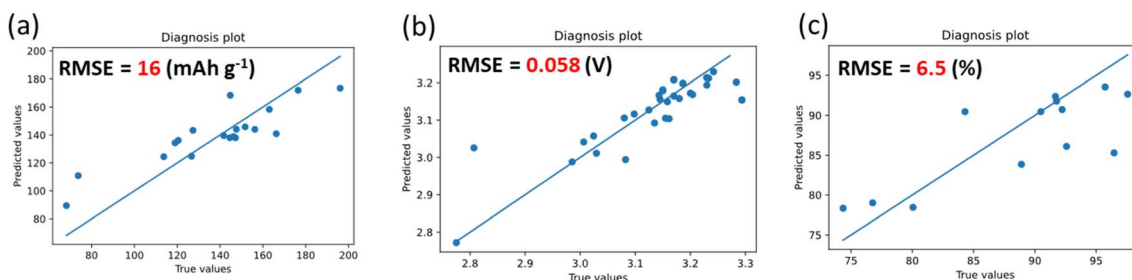

Fig. 2 Test data results of (a) initial discharge capacity, (b) average discharge voltage, and (c) capacity retention at 20th cycle. LightGBM is employed for the discharge capacity and random forest was employed for discharge voltage and capacity retention.

31104 | J. Mater. Chem. A, 2024, 12, 31103–31107

This journal is © The Royal Society of Chemistry 2024

corresponding to an average relative error of 4.0%. Since our dataset contains several charge–discharge data with different voltage ranges for the same composition sample, we also evaluate the prediction capability only for the compositions not contained in training data (Table S2 and Fig. S3†). All models showed similar RMSE even for the new compositions, indicating these models can predict electrochemical performance from the compositions of O3–NaMeO$_2$.

The impact of explanatory variables on objective variables was visualized through shapley additive explanation (SHAP) (Fig. S4†). The potential range have a reasonable impact on all properties. Shortly, a wider voltage range results in higher capacity but lower capacity retention. In predicting initial discharge capacity, excess amounts of Fe, Sn, and Al result in lower capacity, whereas a relatively high Mn or Ni amount tends to lead to high capacity. These results are consistent with the redox inactivity of Sn^{4+} and Al^{3+},[21] and the multi-electron reactions of Mn and Ni.[22,23] In terms of Fe content, a small amount of substitution tended to increase the capacity. However, the excess amount of Fe results in decreased capacity, likely because the migration of Fe in NaFeO$_2$ results in low reversibility and reduced capacity. For the average discharge voltage, Mn and Fe content played a significant role, showing excess Mn and Fe contents lead to lower discharge voltage. In contrast, Sn works to improve the predicted voltage, which is attributed to the addition of Sn enhancing the ionic bonding between oxygen and other transition metals near Sn.[24,25] In the capacity retention model, the Mn and Ni contents are of significant importance, with Mn and Ni demonstrating positive and negative impacts on the prediction values, respectively. This is consistent with a previous report.[5]

The multi-objective optimization search proposed 205 compositions (Fig. 3a). These compositions were distributed between the energy density of positive electrode of 535–563 W h kg^{-1} and capacity retention of 92.3–93.7%. The compositions with high energy density of positive electrode are mainly Ni-rich (∼40%), while the compositions with high capacity retention are Mn-rich (∼60%) (Fig. 3b and c). Then, the composition with the highest predicted active material energy density, NaMn$_{0.3413}$Ni$_{0.4488}$Ti$_{0.1648}$Fe$_{0.04512}$O$_2$ (MNTF), was

targeted for experimental validation. It should be noted that this level of precise compositional optimization is not necessary because of the purity of chemical reagents and experimental errors. Furthermore, the MNTF synthesized in this study contains only a trace amount of Fe. Because it has been reported that even slight variations in Fe amount can affect the initial discharge capacity, operating voltage, and capacity retention rate,[13] we synthesized the material by adding a trace amount of Fe as per the proposed composition and investigated its electrochemical properties.

The synthesized sample was evaluated through synchrotron XRD (SXRD), ICP, and SEM. The SXRD pattern can be fitted well with reasonable R values using the O3-type structure model with $R\bar{3}m$ space group by Rietveld methods (Fig. 4a, Table S3†), indicating that the pure O3 phase was successfully synthesized. The lattice constants were also 0.007 Å longer for the a-axis and 0.076 Å longer for the c-axis compared to those of NaNi$_{0.5}$Mn$_{0.5}$O$_2$.[26] This increase is considered to be due to the substitution of Ti and Fe in NaNi$_{0.5}$Mn$_{0.5}$O$_2$. The ICP measurement showed Na[Mn$_{0.355}$Ni$_{0.442}$Ti$_{0.148}$Fe$_{0.046}$]O$_2$ as the actual composition (Table S4†), closely matching the intended composition. Additionally, SEM images displayed that the MNTF particle size ranged from 0.3–1 μm in diameter (Fig. S5†).

Galvanostatic charge–discharge tests were conducted for the synthesized MNTF electrode in the voltage range of 2.0–4.2 V. The initial discharge capacity of MNTF was 169 mA h g^{-1}, and the average discharge voltage was 3.22 V (Fig. 4b), which agreed with the predicted values of 172 mA h g^{-1} and 3.28 V. However, the experimentally obtained capacity retention at the 20th cycle was 83.0%, which was notably lower than the predicted value of 92.3%. This capacity decay would be attributed to a phase evolution and/or particle cracking of MNTF during charge–discharge reaction, indicated by the voltage plateau at 4.17 V. In our previous reports, NaNi$_{0.5}$Mn$_{0.5}$O$_2$ undergoes a structural change from the P3 structure to the O3 structure with a 22% volume shrinkage during charging at 4.0 V or higher,[26] and the particle size and shape of P2/P3-type Na$_{0.76}$Ni$_{0.38}$Mn$_{0.62}$O$_2$ are important factors determining capacity retention.[27] Thus, it is anticipated that the phase change observed in this study is accompanied by a similar volume change to that of
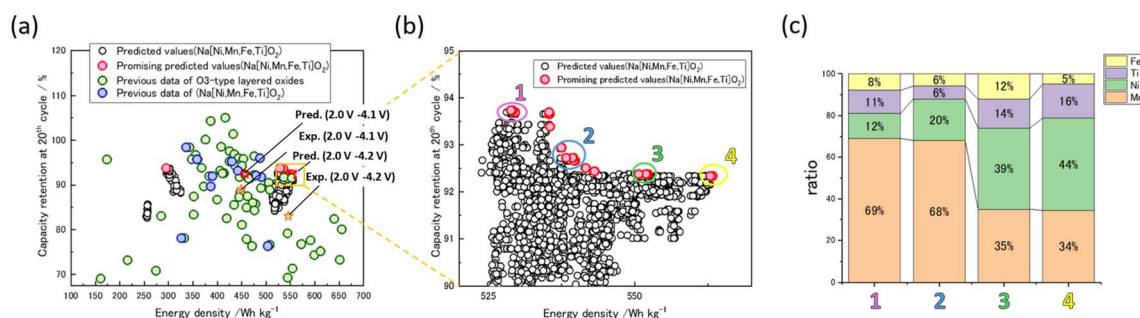

Fig. 3 (a) Comparison of the electrochemical properties of the database used for training and the measured electrochemical properties of the proposed MNTF. Red stars indicate the predicted values at of MNTF at 2.0−4.2 V and 2.0−4.1 V, orange stars indicate the results of charging and discharging MNTF at 2.0−4.2 V, and the results of charging and discharging MNTF at 2.0−4.1 V. (b) An expanded display of the search results, (c) chart depicting the distribution of the proposed 205 promising compositions, categorized into four groups based on their electrochemical properties, each group represented by a representative composition.
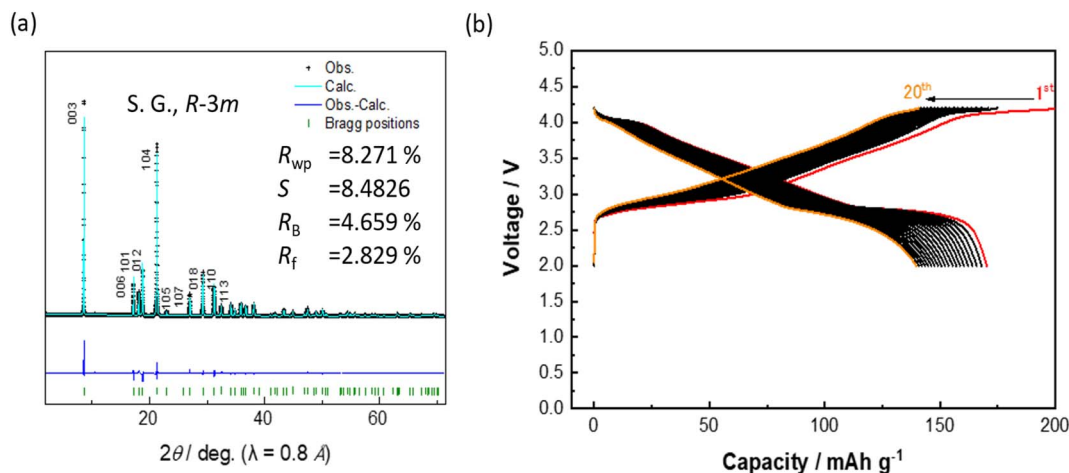
This journal is © The Royal Society of Chemistry 2024

J. Mater. Chem. A, 2024, **12**, 31103–31107 | **31105**

Fig. 4 (a) Rietveld analysis of SXRD data of MNTF and (b) galvanostatic charge and discharge curves for MNTF//Na cells.

$NaNi_{0.5}Mn_{0.5}O_2$.[26] Therefore, charge–discharge tests were further performed within the voltage range of 2.0–4.1 V. The initial discharge capacity was 146 mA h g^{-1}, with an energy density of positive electrode of 449 W h kg^{-1} and a capacity retention of 89.1% after the 20th cycle (Fig. S6†). Capacity retention improved by more than 6 percent point compared to 83% obtained in the range of 2.0–4.2 V. This improvement is believed to be linked to the absence of the phase evolution at 4.17 V. The details of phase evolution are currently under investigation and will be reported elsewhere.

As shown in the above result, charge–discharge voltage ranges significantly affect both the reversible capacity and capacity retention. Thus, the prediction ability of our models in the different voltage ranges is further evaluated for the case of MNTF. The predicted and experimental discharge capacity and energy density of positive electrode obtained from the voltage range of 2.0–4.1 V and 2.0–4.2 V matched closely with the experimental values (Fig. 3, Table S5†). However, the prediction of capacity retention significantly deviated from the experimental value when cycling at 2.0–4.2 V, whereas the prediction for 2.0–4.1 V remained relatively close to the experimental value (Table S5, Fig. S7†). This prediction error indicates that the model does not adequately predict the effects of structural changes on capacity retention. Therefore, incorporating the effects of structural change and particle morphology within the model should be necessary to accurately predict capacity retention.

Finally, the electrochemical performance of MNTF was compared with the data in our dataset. Notably, the MNTF exhibits the highest energy density of positive electrode in the 2.0–4.2 V range among the quaternary (or less) Mn–Ni–Ti–Fe system (Fig. 3a, blue plots). In addition, comparing the energy density achieved by the current material with that reported in the past for O3 NaMeO$_2$ (Fig. S8†). In previous reports, there has been only one instance where energy density exceeded 500 W h per kg of active material. Therefore, the composition synthesized in this study can be considered to have a sufficiently high energy density.[28] Moreover, the methodology and approach utilized in this study can be extendable to more complex systems such as quinary transition metal oxides.

Conclusions

In this study, we predicted the electrochemical properties of O3-type layered oxides from the chemical composition using ML, utilizing experimental data obtained in our group. The predictive model was used to search for potential promising compositions of Ni–Mn–Fe–Ti layered oxides, and we successfully synthesized the suggested O3-type layered oxide of Na[Mn$_{0.36}$Ni$_{0.44}$Ti$_{0.15}$Fe$_{0.05}$]O$_2$. The material showed an initial discharge capacity of 169 mA h g^{-1} and an initial discharge voltage of 3.22 V, in good agreement with the predicted values of 172 mA h g^{-1} and 3.27 V, respectively. The resulting initial energy density of 549 W h per kg of active material was the highest among Na[Ni,Mn,Fe,Ti]O$_2$ samples tested in a voltage range of 2.0–4.2 V in our dataset. On the other hand, lower capacity retention was observed than the predicted values, which can be attributed to the phase evolution around 4.2 V. Thus, improving the prediction ability for capacity retention is essential, and it will be achieved by considering phase evolution during charge–discharge reactions. The approach established in this study offers an efficient method to identify promising compositions from a wide range of potential candidates.

Data availability

The data supporting this article have been included as part of the ESI.† For the data regarding Fig. 2 and 3, we cannot disclose them because they were utilized in model construction through a collaborative research project with a company.

Conflicts of interest

There are no conflicts to declare.

Acknowledgements

31106 | *J. Mater. Chem. A*, 2024, **12**, 31103–31107

This journal is © The Royal Society of Chemistry 2024

References

1 J.-M. Tarascon, Is lithium the new gold?, *Nat. Chem.*, 2010, **2**, 510.

2 I. Hadjipaschalis, A. Poullikkas and V. Efthimiou, Overview of current and future energy storage technologies for electric power applications, *Renew. Sustain. Energy Rev.*, 2009, **13**, 1513–1522.

3 K. Kubota, Electrochemistry and Solid-State Chemistry of Layered Oxides for Li-, Na-, and K-Ion Batteries, *Electrochemistry*, 2020, **88**, 507–514.

4 C. Delmas, C. Fouassier and P. Hagenmuller, Structural classification and properties of the layered oxides, *Phys. B*, 1980, **99**, 81–85.

5 K. Kubota, S. Kumakura, Y. Yoda, K. Kuroki and S. Komaba, Electrochemistry and Solid-State Chemistry of $NaMeO_2$ (Me = 3d Transition Metals), *Adv. Energy Mater.*, 2018, **8**, 1703415.

6 C. Delmas, J. Braconnier, C. Fouassier and P. Hagenmuller, Electrochemical intercalation of sodium in $NaxCoO2$ bronzes, *Solid State Ionics*, 1981, **3–4**, 165–169.

7 Z. Lu and J. R. Dahn, *In Situ* X-Ray Diffraction Study of P2-$Na_{2/3}Ni_{1/3}Mn_{2/3}O_2$, *J. Electrochem. Soc.*, 2001, **148**(11), A1225–A1229.

8 N. Yabuuchi, *et al.*, New O2/P2-type Li-Excess Layered Manganese Oxides as Promising Multi-Functional Electrode Materials for Rechargeable Li/Na Batteries, *Adv. Energy Mater.*, 2014, **4**, 1301453.

9 K. Kubota, N. Yabuuchi, H. Yoshida, M. Dahbi and S. Komaba, Layered oxides as positive electrode materials for Na-ion batteries, *MRS Bull.*, 2014, **39**, 416–422.

10 J.-Y. Hwang, C. S. Yoon, I. Belharouak and Y.-K. Sun, A comprehensive study of the role of transition metals in O3-type layered $Na[Ni_xCo_yMn_z]O_2$ (x = 1/3, 0.5, 0.6, and 0.8) cathodes for sodium-ion batteries, *J. Mater. Chem. A*, 2016, **4**, 17952–17959.

11 K. Kubota, *et al.*, Understanding the Structural Evolution and Redox Mechanism of a $NaFeO_2$-$NaCoO_2$ Solid Solution for Sodium-Ion Batteries, *Adv. Funct. Mater.*, 2016, **26**, 6047–6059.

12 R. Fielden and M. N. Obrovac, Investigation of the $NaNi_xMn_{1-x}O_2$ ($0 \leq x \leq 1$) System for Na-Ion Battery Cathode Materials, *J. Electrochem. Soc.*, 2015, **162**, A453–A459.

13 S. Komaba, Sodium-driven Rechargeable Batteries: An Effort towards Future Energy Storage, *Chem. Lett.*, 2020, **49**, 1507–1516.

14 S. Komaba, *et al.*, Electrochemical Na Insertion and Solid Electrolyte Interphase for Hard-Carbon Electrodes and Application to Na-Ion Batteries, *Adv. Funct. Mater.*, 2011, **21**, 3859–3867.

15 T. Lombardo, *et al.*, Artificial Intelligence Applied to Battery Research: Hype or Reality?, *Chem. Rev.*, 2022, **122**, 10899–10969.

16 M. Harada, *et al.*, Bayesian-optimization-guided experimental search of NASICON-type solid electrolytes for all-solid-state Li-ion batteries, *J. Mater. Chem. A*, 2020, **8**, 15103–15109.

17 N. Kireeva and V. S. Pervov, Materials Informatics Screening of Li-Rich Layered Oxide Cathode Materials with Enhanced Characteristics Using Synthesis Data, *Batter. Supercaps.*, 2020, **3**, 427–438.

18 K. Sodeyama, Y. Igarashi, T. Nakayama, Y. Tateyama and M. Okada, Liquid electrolyte informatics using an exhaustive search with linear regression, *Phys. Chem. Chem. Phys.*, 2018, **20**, 22585–22591.

19 X. Chen, X. Liu, X. Shen and Q. Zhang, Applying Machine Learning to Rechargeable Batteries: From the Microscale to the Macroscale, *Angew. Chem., Int. Ed.*, 2021, **60**, 24354–24366.

20 M. Alipour, S. S. Tavallaey, A. M. Andersson and D. Brandell, Improved Battery Cycle Life Prediction Using a Hybrid Data-Driven Model Incorporating Linear Support Vector Regression and Gaussian, *ChemPhysChem*, 2022, **23**, e202100829.

21 H. Yoshida, *et al.*, P2-type $Na_{2/3}Ni_{1/3}Mn_{2/3-x}Ti_xO_2$ as a new positive electrode for higher energy Na-ion batteries, *Chem. Commun.*, 2014, **50**, 3677–3680.

22 J. U. Choi, J. H. Jo, Y. J. Park, K.-S. Lee and S.-T. Myung, Mn-Rich P′2-Na0.67[Ni0.1Fe0.1Mn0.8]O2 as High-Energy-Density and Long-Life Cathode Material for Sodium-Ion Batteries, *Adv. Energy Mater.*, 2020, **10**, 2001346.

23 J.-Y. Hwang, C. S. Yoon, I. Belharouak and Y.-K. Sun, A comprehensive study of the role of transition metals in O3-type layered $Na[Ni_xCo_yMn_z]O_2$ (x = 1/3, 0.5, 0.6, and 0.8) cathodes for sodium-ion batteries, *J. Mater. Chem. A*, 2016, **4**, 17952–17959.

24 Y. Hu, *et al.*, Sn and Na Co-doping to Suppress Voltage Decay of Li-rich Layered Oxide, *ChemElectroChem*, 2021, **8**, 2315–2320.

25 M. Sathiya, *et al.*, Reversible anionic redox chemistry in high-capacity layered-oxide electrodes, *Nat. Mater.*, 2013, **12**, 827–835.

26 K. Kubota, *et al.*, Impact of Mg and Ti doping in O3 type NaNi 1/2Mn 1/2O2 on reversibility and phase transition during electrochemical Na intercalation, *J. Mater. Chem. A*, 2021, **9**, 12830–12844.

27 E. J. Kim, *et al.*, Effects of Particle Size and Polytype on the Redox Reversibility of the Layered Na0.76Ni0.38Mn0.62O2 Electrode, *ACS Appl. Energy Mater.*, 2024, **7**, 1015–1026.

28 N. Tapia-Ruiz, *et al.*, 2021 roadmap for sodium-ion batteries, *J. Phys. Energy*, 2021, **3**, 031503.